Conference on Modelling Fluid Flow (CMFF'25)
The 19th International Conference on Fluid Flow Technologies
Budapest, Hungary, August 26-August 29, 2025

A Consistent Approach to Atmospheric Boundary Layer Simulations Using the k-ω SST Model

Márton PRICZ[1], Bálint PAPP[2], Gergely KRISTÓF[3] Miklós BALOGH[4],

[1] Corresponding Author. Department of Fluid Mechanics, Faculty of Mechanical Engineering, Budapest University of Technology and Economics, Műegyetem rkp. 3., H-1111 Budapest, Hungary. Tel.: +36 1 463 2546, E-mail: priczmarton@edu.bme.hu
[2] Department of Fluid Mechanics, Faculty of Mechanical Engineering, Budapest University of Technology and Economics. E-mail: papp.balint@gpk.bme.hu
[3] Department of Fluid Mechanics, Faculty of Mechanical Engineering, Budapest University of Technology and Economics. E-mail: kristof.gergely@gpk.bme.hu
[4] Department of Fluid Mechanics, Faculty of Mechanical Engineering, Budapest University of Technology and Economics. E-mail: balogh.miklos@gpk.bme.hu

ABSTRACT

In the computational investigations of atmospheric flows in urban environments, steady-state Reynolds-averaged Navier-Stokes (RANS) simulations are still preferred to transient scale-resolving ones due to their relatively low computational demand and fast turnover times. An extensively documented challenge associated with RANS models in atmospheric applications is the unwanted alteration of the prescribed velocity and turbulence profiles in the streamwise direction, caused by the inadequate treatment of solid wall boundaries and the well-known inconsistencies between the atmospheric boundary layer (ABL) profiles and general-purpose turbulence models. Although several methods have been proposed to preserve the streamwise homogeneity of the neutral ABL, previously, most of these have been developed for the k-ε model family, which is known to perform poorly in impinging and separated flows, making its applicability in building aerodynamics questionable. The present work proposes and benchmarks two approaches, namely custom wall functions and the sand-grain-roughness-based boundary condition, aimed at maintaining the prescribed atmospheric boundary layer inlet profiles in steady-state calculations using the k-ω SST model, which is better suited for investigating flows around bluff bodies. The same approaches are also applied to the standard k-ε and realizable k-ε models for comparison. The proposed methods are implemented in both Ansys Fluent and OpenFOAM and the results from a test case with a surface-mounted cube are compared. Simulations in an empty domain show significant improvements in the homogeneity of the ABL, with the best performance achieved by a logarithmic atmospheric wall function formulation. The accuracy of the proposed methods is quantified by reproducing the surface pressure distribution of a cuboid building model subjected to an ABL-like approach flow in a wind tunnel.

Keywords: Atmospheric boundary layer, Ansys Fluent, k-ω SST, OpenFOAM, Surface-mounted cube, Wall function

NOMENCLATURE

a_b	$[-]$	blending function parameter
A_k	$[m^2/s^2]$	TKE profile parameter
B_k	$[m^2/s^2]$	TKE profile parameter
C_k	$[m^2/s^2]$	TKE profile parameter
c_p	$[-]$	static pressure coefficient
C_s	$[-]$	roughness constant
C_μ	$[-]$	turbulence model constant
D_k	$[m^2/s^2]$	TKE profile parameter
E	$[-]$	empirical constant
f_b	$[-]$	blending function
H	$[m]$	height of the cube
k	$[m^2/s^2]$	turbulent kinetic energy
K_s	$[m]$	sand-grain roughness height
N	$[-]$	number of pressure probes
O	$[-]$	observed (measured) data set
P	$[-]$	predicted (simulated) data set
p	$[Pa]$	static pressure
q	$[-]$	hit rate
R	$[-]$	correlation coefficient
u	$[m/s]$	x-velocity
u^*	$[m/s]$	friction velocity
v	$[m/s]$	y-velocity
w	$[m/s]$	z-velocity
z	$[m]$	vertical coordinate
z_{0k}	$[m]$	TKE profile reference height
z_{0w}	$[m]$	aerodynamic roughness height
z_0	$[m]$	aerodynamic roughness height
z_{mod}	$[m]$	modified vertical coordinate

α	$[-]$	power-law exponent
β^*	$[-]$	turbulence model constant
δ	$[m]$	boundary layer depth
Δ_{abs}	$[-]$	absolute error
Δ_{rel}	$[-]$	relative error
κ	$[-]$	von Kármán constant
ν	$[m^2/s]$	kinematic viscosity
ω	$[1/s]$	specific dissipation rate
ρ	$[kg/m^3]$	density
σ	$[-]$	standard deviation
τ	$[Pa]$	wall shear stress
ε	$[m^2/s^3]$	turbulence dissipation rate

Subscripts and Superscripts

i	element index of the observed and measured data sets
in	inlet variables
w	values used in the wall function
p	values at the first cell centre
ref	reference values
$+$	nondimensional values

1. INTRODUCTION

A crucial challenge in using Reynolds-averaged Navier-Stokes (RANS) models in atmospheric simulations is creating a so-called horizontally homogeneous atmospheric boundary layer (HHABL) flow by avoiding the unintended streamwise alteration of the prescribed velocity and turbulent kinetic energy profiles as they travel along the numerical domain. This alteration otherwise results in a mismatch between the inflow and approach flow profiles and the flow reaching the area of interest will therefore be different to the intended one – which is a well-documented problem, impacting the fidelity of numerical simulations [1, 2, 3, 4]. This problem stems from the formation of an internal near-wall boundary layer due to inconsistencies between the wall treatment, the transport equations and the inflow profiles[1, 4, 5].

Several studies have proposed methods for the preservation of the inflow profiles of a neutral ABL when using the k-ε model family. These include the modification of model constants [4, 6, 7, 8], the use of corrective source terms [4, 7, 8, 9], and custom wall functions [4, 7, 8, 10] among others. However, the commonly used standard and realizable k-ε models are known to underperform in wall-bounded flows compared to the k-ω SST model [11]. This is apparent in flows around bluff bodies, where the overprediction of k by the k-ε models reduces or even eliminates the separation behind the windward edges of obstacles [11, 12, 13]. The k-ω SST model performs significantly better in impinging and separated flows, making it a preferable alternative for bluff body flow simulations [11].

However, the commonly used Ansys Fluent CFD solver – hereinafter referred to as Fluent – does not provide an option to employ user-defined wall functions when using ω-based turbulence models. Instead, the user must rely on the rough wall boundary condition based on the sand grain roughness model. While formulations for a consistent set of roughness parameters and inlet conditions have already been proposed, these either rely on the drastic modification of model constants [14], or must employ overly large cells near the wall to abide by the requirements for creating a HHABL flow, originally formulated by Blocken et al. [3] [15]. As an example, the optimal set of roughness parameters for a high-roughness ABL flow determined by Townsend et al. [15] requires roughly $29\,m$ high first cells at full scale, which is in itself larger than many low-rise buildings.

The current work proposes a new formulation for obtaining an optimum set of roughness parameters using this boundary condition and shows how the well-known contradiction in the requirements for a high-fidelity HHABL simulation [3] can be circumvented with the current version of Fluent (version 2023 R1). Comparisons are drawn between the applicable wall treatment methods in OpenFOAM and Ansys Fluent as well as between the implementations available for the k-ε and k-ω SST models. The performance of the new method for prescribing appropriate surface roughness for neutral HHABL flows is assessed based on the velocity and TKE profiles in a two-dimensional empty channel and the surface pressure distribution of a surface-mounted cube in a three-dimensional channel.

2. METHODOLOGY

2.1. Inflow conditions

The inlet boundary conditions are determined based on the wind tunnel measurements of [16], with auxiliary data supplemented from [17] and are identical in the OpenFOAM and Fluent simulations. A neutrally stratified, hydrostatic ABL is assumed, where the balancing buoyant and gravitational forces are subtracted from the equation of motion, and the problem is regarded as incompressible. The thermal stratification is therefore not considered in this work. For the velocity profile, a power-law function is fitted to the entire data set. A horizontally homogeneous flow is assumed, with zero mean vertical and lateral velocity components ($v \equiv 0; w \equiv 0$), in the form of

$$u(z) = u_{ref}\left(\frac{z + z_{ref}}{z_{ref}}\right)^{\alpha} - u_{ref}, \tag{1}$$

where u_{ref} denotes the reference velocity, z_{ref} is the reference height and α is the exponent of the power-law profile. For the fitted values of the above parameters, see Table 1.

A four-parameter logarithmic-polynomial profile is used for the turbulent kinetic energy (TKE) profile. This generally offers more flexibility for fitting to wind tunnel data than the commonly used profile proposed by Parente et al. [7] and ensures a zero

Table 1. Fitted parameters for the power law and logarithmic mean x-velocity profiles, the logarithmic-polynomial TKE profile and the f_b blending function.

u_{ref} $[m/s]$	z_{ref} $[m]$	α $[-]$	u_w^* $[m/s]$ (Fluent)	u_w^* $[m/s]$ (OpenFOAM)	z_{0w} $[m]$	
0.4472	1.493×10^{-5}	0.2707	0.3839	0.3759	1.060×10^{-3}	
z_{0k} $[m]$	A_k $\left[m^2/s^2\right]$	B_k $\left[m^2/s^2\right]$	C_k $\left[m^2/s^2\right]$	D_k $\left[m^2/s^2\right]$	δ $[m]$	a_b $[-]$
5×10^{-3}	0.1149	-5.453×10^{-2}	5.699×10^{-3}	0.4912	0.4819	7.591

gradient at the wall [18]:

$$k(z) = A_k \ln^2\left(\frac{z+z_{0k}}{z_{0k}}\right) + B_k \ln^3\left(\frac{z+z_{0k}}{z_{0k}}\right) + C_k \ln^4\left(\frac{z+z_{0k}}{z_{0k}}\right) + D_k, \tag{2}$$

where the value of z_{0k}, A_k, B_k, C_k and D_k parameters are listed in Table 1. The inflow profiles of ε and ω for the respective RANS models are determined based on the profiles of u and k:

$$\varepsilon(z) = \sqrt{C_\mu} k(z) \frac{\partial u(z)}{\partial z} \tag{3}$$

and ω can be expressed from ε via the transformation of Wilcox [19], adopted by Menter [20]:

$$\omega(z) = \frac{\varepsilon(z)}{\beta^* k(z)} = \frac{1}{\sqrt{C_\mu}} \frac{\partial u(z)}{\partial z}, \tag{4}$$

where β^* and C_μ model constants are both kept at the Fluent default value of 0.09 [18].

In the wind tunnel measurements, the appropriate velocity profile was created using physical obstacles, including tripping fences and turbulence-generating spires. These elements did not extend to the top of the wind tunnel and the flow above them remained uniform. To model this effect, a modified z_{mod} vertical coordinate is introduced, expressed as

$$z_{mod}(z) = z(1 - f_b(z)) + \delta f_b(z), \tag{5}$$

where δ is the depth of the boundary layer in the wind tunnel and $f_b(z)$ is given as

$$f_b(z) = \frac{1}{2}\left(1 + \sin\left(\frac{\pi}{2} \max\left(-1, \min\left(a_b(z-\delta), 1\right)\right)\right)\right), \tag{6}$$

where a_b is a fitted blending parameter. The values of δ and a_b are listed in Table 1.

2.2. Wall treatment

2.2.1. Wall treatment in OpenFOAM

In the case of the OpenFOAM simulations, a logarithmic law of the wall is employed. The friction velocity u_w^* and aerodynamic roughness height z_{0w} in Equation 7 are determined by fitting a logarithmic profile to the velocity measurements in the range of $4 \times 10^{-3}\, m < z < 6 \times 10^{-2}\, m$.

$$U_w(z) = \frac{u_w^*}{\kappa} \log\left(\frac{z+z_{0w}}{z_{0w}}\right), \tag{7}$$

where κ is the von Kármán constant, with slightly different default values in the two solvers (OpenFOAM: $\kappa = 0.41$, Fluent: $\kappa = 0.4187$), hence the different friction velocities used in the implementations in the respective solver (see Table 1).

2.2.2. Wall treatment in Fluent

As mentioned in Section 1, user-defined wall functions are not available for the k-ω SST model in Fluent. Therefore, the logarithmic wall function is only used with the standard k-ε and realizable k-ε models, while the rough wall condition is used for the k-ω SST model instead. For fully rough boundary layers – as is the case in ABL flows in general – the velocity in the first cell centre next to the wall is calculated as

$$\frac{u_p u^*}{\tau_w/\rho} = \frac{1}{\kappa} \ln\left(\frac{E z_p^+}{1 + C_s K_s^+}\right), \tag{8}$$

where, from here on, subscript p denotes the values in the first cell centre, at the height of $z = z_p$. Furthermore, $E = 9.793$ is an empirical constant, $u^* = C_\mu^{1/4} k_p^{1/2}$ is the friction velocity, τ_w is the wall shear stress, ρ is the density of the fluid and the C_s roughness constant and K_s sand grain roughness height are provided by the user. The z_p^+ and K_s^+ values are nondimensionalized as $z_p^+ = z_p u^*/\nu$ and $K_s^+ = K_s u^*/\nu$ respectively, where ν is the kinematic viscosity. In the current work, the value of C_s is kept constant (at the Fluent default value of 0.5 [21]), while K_s is chosen so that Eqs. (7) and (8) give the same velocity values for the first cell centre, meaning

$$\frac{\tau_w/\rho}{u^*} \frac{1}{\kappa} \ln\left(\frac{E z_p^+}{1 + C_s K_s^+}\right) = \frac{u_w^*}{\kappa} \log\left(\frac{z+z_{0w}}{z_{0w}}\right). \tag{9}$$

By rearranging Eq. (9), the roughness height can be expressed as

$$K_s = \frac{E z_p z_{0w}}{C_s\left(z_p + z_{0w}\right)} - \frac{1}{C_s^+}, \tag{10}$$

where C_s^+ contains the approximate values of the various formulations of the friction velocity found in

Eqs. (7) and (8):

$$C_s^+ = \frac{\tau_w/\rho}{u^* \nu} C_s \approx \frac{\nu \frac{\mathrm{d}U}{\mathrm{d}z}\Big|_{z_p} + C_\mu^{1/2} k_p}{C_\mu^{1/4} k_p^{1/2} \nu} C_s. \tag{11}$$

With C_s being fixed at 0.5, the resulting roughness height is $K_s = 3.818 \times 10^{-3}\, m$. This value is higher than the first cell centre height $z_p = 3 \times 10^{-3}\, m$ and therefore does not satisfy the minimum cell height criterion formulated by Blocken et al. [3]. However, the authors noted that this limitation was posed by the available 6.2 version of Fluent at the time, and in case of future developments in this regard, this requirement might need to be reconsidered. Indeed, since version 14, Fluent does not restrict the wall-normal mesh resolution based on the roughness height (see section 7.4.15.3.1 in the Ansys Fluent User's Guide [21]). Thus the above-presented parameter values can be employed with no apparent conflict.

2.3. Numerical setup

2.3.1. Empty channel

The wall functions and optimized roughness parameters are first assessed using a two-dimensional empty channel with a length of $1.2\, m$ and a height of $1\, m$, matching the wind tunnel in the experimental investigations [16]. (While this domain will be referred to as a two-dimensional, it is effectively a single-cell-wide three-dimensional domain, as OpenFOAM uses three-dimensional meshes exclusively. For a direct comparison of the results, the same mesh is employed in Fluent.) The numerical mesh consists of 6360 (60×106) hexahedral cells, with uniform horizontal spacing, a first cell layer height of $6 \times 10^{-3}\, m$ and a wall-normal grading with a reference cell expansion ratio of 1.14.

The inflow profiles described in Section 2.1 are imposed at the inlet, while zero gauge pressure is prescribed at the outlet. The wall treatment methods are applied to the channel floor, and a symmetry condition is applied to the top boundary. In the OpenFOAM implementation of the 2D channel, the lateral boundaries are set to "empty", while a symmetry condition is applied to them in Fluent.

2.3.2. Surface-mounted cube

After the preliminary 2D simulations, the methods are employed for a 3D channel containing a surface-mounted cube with an edge length of $H = 0.2\, m$. The vertical and lateral dimensions of the domain match the cross-section of the wind tunnel, while the longitudinal dimensions upwind and downwind of the cube are set in accordance with the guidelines of Franke et al. [22]. For the domain dimension, see Figure 1. The mesh is fully structured and uses the same first cell height and vertical grading as the 2D mesh outside the vicinity of the cube, resulting in 1.15 million hexahedral cells. At the surface of the cube, 26 cells are located along the horizontal edges and 23 along the vertical edges. The

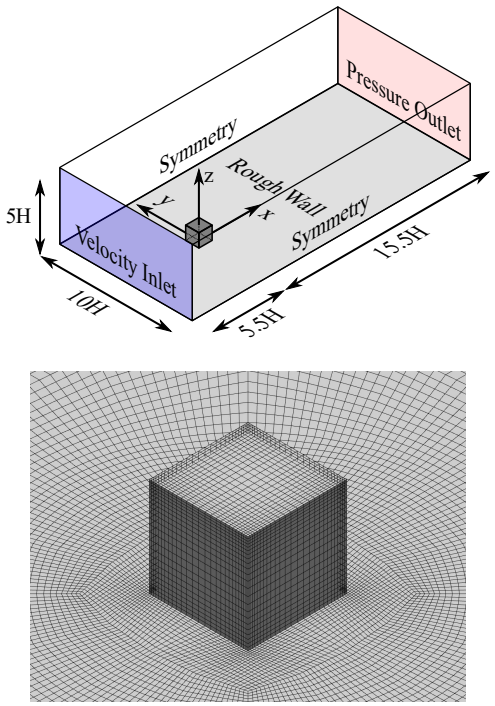

Figure 1. Top: sketch of the 3D computational domain with the surface-mounted cube. Dimensions are displayed relative to the cube height ($H = 0.2\, m$). Bottom: close-up image of the mesh at the surface of the cube.

3D simulation uses the same boundary conditions as the 2D channel, except for the "empty" conditions at the lateral boundaries in OpenFOAM, which are replaced by the slip wall boundary condition. Additionally, the faces of the cube are treated as smooth walls.

2.3.3. Solver settings

Air density was set to $1\, kg/m^3$ and the kinematic viscosity accordingly to $1.5 \times 10^{-5}\, m^2/s$ in the Fluent simulations for direct compatibility with the OpenFOAM calculations. (OpenFOAM solves for the kinematic pressure p/ρ instead of the static pressure in incompressible cases, assuming unit density.)

Table 2. Naming convention of cases. The last character denotes the solver used in the specific case (O– OpenFOAM, F– Fluent)

Notation	Turbulence model	Wall treatment
SSTKW-F	k-ω SST	Rough wall
SSTKW-O	k-ω SST	Log-law
SKE-F	Standard k-ε	Log-law
SKE-O	Standard k-ε	Log-law
RKE-F	Realizable k-ε	Log-law
RKE-O	Realizable k-ε	Log-law

The simulations were performed using steady-state incompressible solvers in both software with a second-order spatial discretization of the pres-

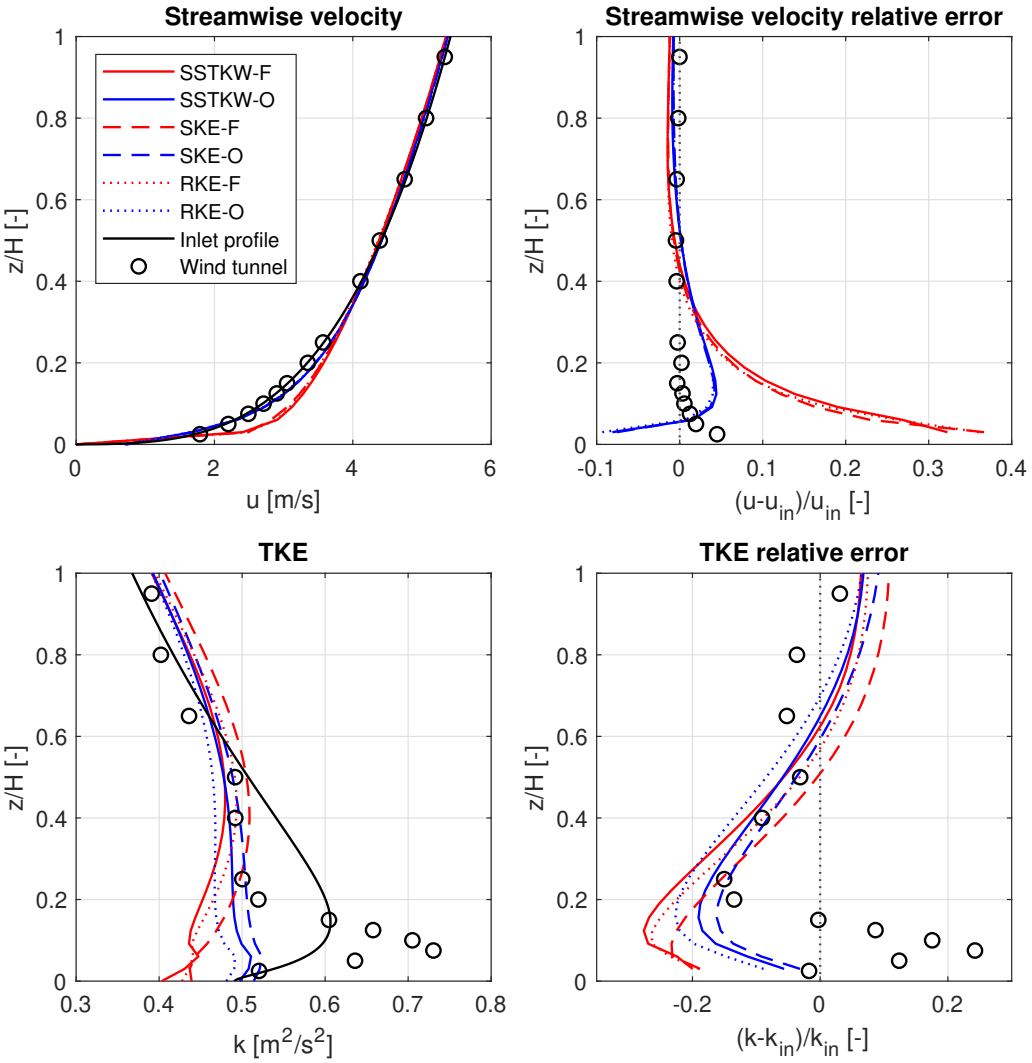

Figure 2. Vertical profiles of u (top) and k (bottom) with their relative errors to the prescribed inlet profiles below $z = H$ height at the outlet, with a distance of $x = 6H$ from the inlet.

sure, second-order upwind discretization for the momentum and first-order upwind discretization for the turbulent variables. All 3D simulations are performed on the CPU partition of the Komondor High-Performance Computer (HPC), using 24 processor cores of an AMD EPYC™ 7763 processor.

3. RESULTS

3.1. Empty channel

The velocity and its relative error at the outlet (at $x = 6H$) of the 2D channel (Figure 2) show that all five implementations utilizing a logarithmic wall function behave similarly, with error values generally below 10% in the most critical, near-ground region. Out of these cases, those using the standard k-ε model produce the highest relative error at the first cell centre, at 9.6% and 9.3% for the Fluent and OpenFOAM implementations respectively. It should also be noted, that the OpenFOAM simulations using the standard and realizable k-ε models result in marginally smaller relative errors than their counterparts in Fluent (average absolute deviations from the prescribed profile below $z = H$: SKE-F - 2.02%, SKE-O - 1.70%, RKE-F - 1.88% and RKE-O - 1.74%). Meanwhile, the rough wall implementation in Fluent (case SSTKW-F) produces noticeably larger errors at almost all locations below $z = H$, with a peak relative error of 32.3% immediately next to the wall (average absolute deviations from the prescribed profile below $z = H$: SSTKW-F - 5.49% and SSTKW-O - 1.84%). This points to the rough wall function behaving differently to the formulation shown in Eq. 8, likely due to the compensation for the cell centre height being smaller than the roughness height [21]. This produces a different velocity at the first cell centre compared to the other simulations, indicating that the local near-wall speedup of the flow may still compromise the results at this height.

The resulting TKE profiles at the outlet show considerable deviations from the inlet profile in all cases. The maximum relative errors to the fitted profile range from 16.19% to 24.61%, with the highest

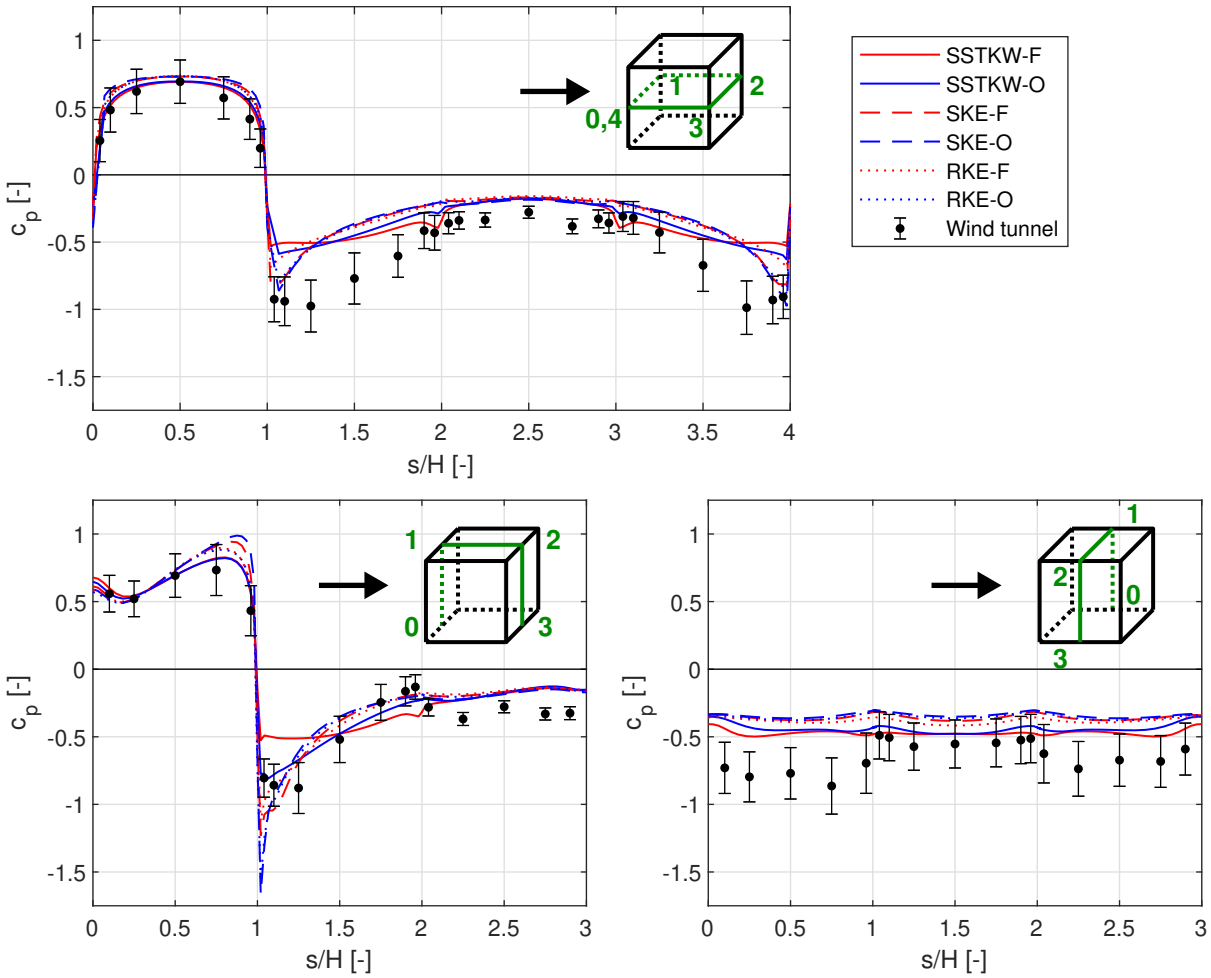

Figure 3. Distribution of the pressure coefficient along the horizontal and vertical centre lines of the cube. Error bars correspond to rms measurement values. s/H denotes the nondimensional distance along the centre lines. (For the orientation, see the sketches in the top right corners of the plots, where the black arrow shows the wind direction.)

error once again produced by the SSTKW-F case, using the rough wall condition. Despite the improved formulation of the TKE profile, the fit to the experimental data is far from ideal and the measured values themselves deviate from this profile considerably, with errors comparable to those produced by the simulations.

3.2. Surface-mounted cube

The results of the simulations in the three-dimensional domain are validated with the experimental surface pressure data from [16]. For this purpose, the static pressure values are presented as pressure coefficients, calculated as

$$c_p = \frac{p - p_0}{\frac{1}{2}\rho u_H^2}, \tag{12}$$

where $u_H = 5.412\,m/s$ is the prescribed inflow velocity at $z = H$ and the p_0 reference static pressure is sampled in the numerical domain at the same location as in the measurement; at the channel wall, in the lateral midplane of the cube and at the height of 0.25 m.

Figure 3 shows the distribution of the pressure coefficient along the horizontal and vertical centre lines of the cube. The depression on the sides of the cube (s/H between 1-2 and 3-4 in the top plot of Figure 3) is underpredicted by both k-ω SST simulations, while it is only significantly underpredicted behind the top leading edge ($s/H = 1$ in the bottom left plot of Figure 3) by the Fluent implementation of the k-ω SST model. As this location is sufficiently far from the channel floor, it is likely that this discrepancy between the two simulations is not the result of the different wall treatment methods but rather a difference in the implementations of the k-ω SST model itself in the two solvers. The Fluent and OpenFOAM simulations, which use the standard k-ε and realizable k-ε models, produce largely similar pressure distributions, invariably overestimating the magnitude of the front overpressure and the depression behind the top leading edge. All turbulence models generally overestimate the pressure on the windward, side and leeward walls, with the most noticeable deviations from the experimental data shown on

the side walls. Overall, the k-ω SST cases, and specifically the SSTKW-O case provide the best agreement between the simulated and measured values.

Following the qualitative remarks, four different scalar metrics were employed to provide a basis for comparing the performance of the individual implementations quantitatively. These are the correlation coefficient (R), the hit rate (corresponding to the value of the measurement uncertainty, $q_{0.142}$), the factor of two observations ($FAC2$) and the average absolute deviation (AAD). Their calculation is as follows:

$$R = \frac{\overline{\left(O_i - \overline{O}\right)\left(P_i - \overline{P}\right)}}{\sigma_O \sigma_P} \tag{13}$$

$$q = \frac{1}{N}\sum_{i=1}^{N} n_i, \text{ where}$$
$$n_i = \begin{cases} 1 & \text{if} \quad (1 - \Delta_{rel}) \leq \frac{P_i}{O_i} \leq (1 + \Delta_{rel}) \\ 1 & \text{if} \quad |P_i - O_i| < \Delta_{abs} \\ 0 & \text{otherwise,} \end{cases} \tag{14}$$

$$FAC2 = \frac{1}{N}\sum_{i=1}^{N} n_i, \text{ where}$$
$$n_i = \begin{cases} 1 & \text{if} \quad 0.5 \leq \frac{P_i}{O_i} \leq 2 \\ 1 & \text{if} \quad |P_i| < \Delta_{abs} \text{ and } |O_i| < \Delta_{abs} \\ 0 & \text{otherwise,} \end{cases} \tag{15}$$

and

$$AAD = \overline{|O_i - P_i|}. \tag{16}$$

In the above definitions, O_i and P_i respectively denote observed (measured) and predicted (simulated) pressure coefficient values at the i^{th} static pressure tap on the surface of the cube, with σ_O and σ_P denoting the standard deviation of the observed and predicted dataset, the overbars above quantities denoting mean values and $N = 175$ standing for the total number of pressure taps on the surface of the cube. For the arrangement of the pressure taps, the reader is referred to Papp et al. [16]. Furthermore, $\Delta_{abs} = 0.142$ and $\Delta_{rel} = 0.25$ absolute and relative errors are taken from the experimental investigations.

A high correlation coefficient serves as a necessary but not sufficient condition for a good statistical match. This condition is satisfied by all simulations, with values of R ranging from 0.921 to 0.957. However, a simulated pressure distribution achieving a higher correlation coefficient than another does not automatically constitute a better overall agreement with the measurement data. The hit rate and the $FAC2$ metrics are calculated on a similar basis but the latter is generally more robust as it is not affected by outliers. It should also be noted, that assuming smaller errors for the experimental results would automatically narrow the criterion for a "hit" ($n_i = 1$ in Equation 14), leading to a lower hit rate, indicating a worse match between the otherwise unchanged experimental and simulated data.

Table 3. Validation metrics of the surface-mounted cube simulations.

Case	R	$q_{0.142}$	$FAC2$	AAD
SSTKW-F	0.935	0.583	0.909	0.184
SSTKW-O	**0.955**	**0.606**	**0.966**	**0.161**
SKE-F	0.954	0.463	0.886	0.180
SKE-O	0.921	0.451	0.869	0.206
RKE-F	0.957	0.463	0.886	0.186
RKE-O	0.932	0.457	0.903	0.192
Target values	1	1	1	0

The validation metrics show that the SSTKW-O case outperforms all other simulations, with the second-best match achieved by the SSTKW-F case in the hit rate and $FAC2$ metrics. In comparison, the validation metrics generally indicate that the k-ε simulations underperform, with the Fluent implementations achieving somewhat higher hit rates and lower average absolute deviation values than the OpenFOAM cases, although the same trend is not present for the FAC2 metric.

4. CONCLUSIONS

The various implementations of the logarithmic wall functions produced similar results in the empty channel simulations, with maximum relative error values for the velocity consistently below 10%, achieving a good match between the inflow and outflow profiles. The rough wall formulation (necessitated by the limited wall function capabilities of Ansys Fluent) produced the largest velocity errors next to the wall, which points to further improvements needed regarding this method. Meanwhile, the errors in the TKE profiles were significantly higher in every case and the distinction between the performance of the logarithmic wall function and the rough wall function became less clear. The pressure distribution on the surface of the surface-mounted cube shows the clear advantages of using the k-ω SST model, which achieved a better match to the experimental data. Based on the employed validation metrics, the best overall agreement with the experimental data was achieved by the OpenFOAM implementation of the k-ω SST model, with significant differences noted between the behaviour of the Fluent and OpenFOAM implementations.

ACKNOWLEDGEMENTS

The authors would like to thank the Digital Government Development and Project Management Ltd. for awarding them access to the Komondor HPC facility based in Hungary. This study was funded by grant no. OTKA K23-146158 from the National Re-

search, Development, and Innovation Office, Hungary. Project no. TKP-6-6/PALY-2021 has been implemented with the support provided by the Ministry of Culture and Innovation of Hungary from the National Research, Development and Innovation Fund, financed under the TKP2021-NVA funding scheme. The work of Bálint Papp was supported by the EKÖP-24-4-I-BME-357 University Research Scholarship Program of the Ministry for Culture and Innovation, from the source of the National Research Development and Innovation Fund.

REFERENCES

[1] Richards, P. J., and Hoxey, R. P., 1993, "Appropriate boundary conditions for computational wind engineering models using the k-ε turbulence model", *Journal of Wind Engineering and Industrial Aerodynamics*, Vol. 46-47, pp. 145–153.

[2] Hargreaves, D. M., and Wright, N. G., 2007, "On the use of the k-ε model in commercial CFD software to model the neutral atmospheric boundary layer", *Journal of Wind Engineering and Industrial Aerodynamics*, Vol. 95 (5), pp. 355–369.

[3] Blocken, B., Carmeliet, J., and Stathopoulos, T., 2007, "CFD simulation of the atmospheric boundary layer: wall function problems", *Atmospheric Environment*, Vol. 41 (2), pp. 238–252.

[4] Parente, A., Gorlé, C., van Beeck, J., and Benocci, C., 2011, "A Comprehensive Modelling Approach for the Neutral Atmospheric Boundary Layer: Consistent Inflow Conditions, Wall Function and Turbulence Model", *Boundary-Layer Meteorol*, Vol. 140 (3), pp. 411–428.

[5] Richards, P. J., and Norris, S. E., 2019, "Appropriate boundary conditions for computational wind engineering: Still an issue after 25 years", *Journal of Wind Engineering and Industrial Aerodynamics*, Vol. 190, pp. 245–255.

[6] Gorlé, C., van Beeck, J., Rambaud, P., and Van Tendeloo, G., 2009, "CFD modelling of small particle dispersion: The influence of the turbulence kinetic energy in the atmospheric boundary layer", *Atmospheric Environment*, Vol. 43 (3), pp. 673–681.

[7] Parente, A., Gorlé, C., van Beeck, J., and Benocci, C., 2011, "Improved k-ε model and wall function formulation for the RANS simulation of ABL flows", *Journal of Wind Engineering and Industrial Aerodynamics*, Vol. 99 (4), pp. 267–278.

[8] Balogh, M., Parente, A., and Benocci, C., 2012, "RANS simulation of ABL flow over complex terrains applying an Enhanced k-ε model and wall function formulation: Implementation and comparison for fluent and OpenFOAM", *Journal of Wind Engineering and Industrial Aerodynamics*, Vol. 104-106, pp. 360–368.

[9] Balogh, M., and Parente, A., 2015, "Realistic boundary conditions for the simulation of atmospheric boundary layer flows using an improved k-ε model", *Journal of Wind Engineering and Industrial Aerodynamics*, Vol. 144, pp. 183–190.

[10] Chang, C.-Y., Schmidt, J., Dörenkämper, M., and Stoevesandt, B., 2018, "A consistent steady state CFD simulation method for stratified atmospheric boundary layer flows", *Journal of Wind Engineering and Industrial Aerodynamics*, Vol. 172, pp. 55–67.

[11] Cindori, M., Čajić, P., Džijan, I., Juretić, F., and Kozmar, H., 2022, "A comparison of major steady RANS approaches to engineering ABL simulations", *Journal of Wind Engineering and Industrial Aerodynamics*, Vol. 221, p. 104867.

[12] Gao, Y., and Chow, W. K., 2005, "Numerical studies on air flow around a cube", *Journal of Wind Engineering and Industrial Aerodynamics*, Vol. 93 (2), pp. 115–135.

[13] Blocken, B., 2018, "LES over RANS in building simulation for outdoor and indoor applications: A foregone conclusion?", *Build Simul*, Vol. 11 (5), pp. 821–870.

[14] Yang, Y., Xie, Z., and Gu, M., 2017, "Consistent inflow boundary conditions for modelling the neutral equilibrium atmospheric boundary layer for the SST k-ω model", *Wind and Structures*, Vol. 24 (5), pp. 465–480, publisher: Techno-Press.

[15] Townsend, J. F., Xu, G., and Jin, Y., 2024, "Roughness constant selection for atmospheric boundary layer simulations using a *k-ω* SST turbulence model within a commercial CFD solver", *Advances in Wind Engineering*, Vol. 1 (1), p. 100005.

[16] Papp, B., Kristóf, G., and Gromke, C., 2021, "Application and assessment of a GPU-based LES method for predicting dynamic wind loads on buildings", *Journal of Wind Engineering and Industrial Aerodynamics*, Vol. 217, p. 104739.

[17] Gromke, C., and Ruck, B., 2005, "Die Simulation atmosphärischer Grenzschichten in Windkanälen", *Proceedings of the 13 GALA Fachtagung "Lasermethoden in der*

Strömungsmesstechnik", 6-8 September 2005, Cottbus, Germany, pp. 1–8.

[18] ANSYS Inc., Canonsburg, PA, 2023, *Ansys Fluent Theory Guide*, release 2023 R1.

[19] Wilcox, D. C., 1988, "Reassessment of the scale-determining equation for advanced turbulence models", *AIAA Journal*, Vol. 26, pp. 1299–1310, aDS Bibcode: 1988AIAAJ..26.1299W.

[20] Menter, F., 1993, "Zonal two equation kw turbulence models for aerodynamic flows", *23rd fluid dynamics, plasmadynamics, and lasers conference*, p. 2906.

[21] ANSYS Inc., Canonsburg, PA, 2023, *Ansys Fluent User's Guide*, release 2023 R1.

[22] Franke, J., Hellsten, A., Schlunzen, K. H., and Carissimo, B., 2011, "The COST 732 Best Practice Guideline for CFD simulation of flows in the urban environment: a summary", *International Journal of Environment and Pollution*, Vol. 44 (1-4), pp. 419–427, publisher: Inderscience Publishers.